Early-age deformation of hydrophobized metakaolin-based geopolymers

Shengqian Ruan[a,c], Shikun Chen[a], Yi Liu[b], Yajun Zhang[a], Dongming Yan[a,*], Mingzhong Zhang[c,*]

[a] *College of Civil Engineering and Architecture, Zhejiang University, Hangzhou 310058, China.*

[b] *School of Materials Science and Engineering, Zhejiang University, Hangzhou 310027, China.*

[c] *Department of Civil, Environmental and Geomatic Engineering, University College London, London WC1E 6BT, UK*

**Corresponding authors. E-mail addresses: dmyan@zju.edu.cn (D. Yan), mingzhong.zhang@ucl.ac.uk (M. Zhang)*

Abstract: This study presents a novel strategy to simultaneously mitigate the early-age shrinkage and achieve hydrophobization of metakaolin-based geopolymer (MKG) pastes through the incorporation of organic admixtures including polydimethylsiloxane (PDMS) and sodium methylsilicate (SMS). The pore structure, wettability, moisture/water adsorption capacity, and internal moisture distribution are investigated through different techniques including MIP and LF-NMR. Results indicate that the autogenous shrinkage of MKG paste is reduced by 91.2% and 41.6% when adding 5% PDMS and replacing with 20% SMS, and the water contact angle increases to approximately 130° and 140°, respectively. The addition of organic admixtures significantly reduces the moisture adsorption and surface tension of MKG matrix, and thus internal water tends to be transported into larger pores, leading to less liquid-vapor meniscus and lower capillary stress. Moreover, an underlying mechanism is proposed to explain the shrinkage mitigation of hydrophobized MKG paste, accounting for the moisture transfer tendency and internal stress distribution.

Keywords: Geopolymer; Hydrophobic modification; Autogenous shrinkage; Pore size distribution; Moisture distribution

1. Introduction

Geopolymers are a class of aluminosilicate-rich inorganic materials which have been regarded as potential alternatives to Portland cement (PC) because of their superior mechanical properties and thermal stability as well as low carbon footprint [1-5]. Geopolymers tend to undergo obvious volume changes during early-age curing, which is an important factor affecting their durability. The common types of early-age deformation (shrinkage or expansion) include chemical and autogenous deformations. The chemical deformation refers to the volume change caused by the difference in average density between reaction products (e.g., sodium aluminosilicate hydrate gels for metakaolin-

based geopolymers (MKG)) and fresh aluminosilicate paste during geopolymerization [6-7]. The autogenous deformation is defined as the macroscopic volume change caused by the microstructure change and capillary negative pressure under the premise of no material exchange and no external force, which mainly includes chemical deformation and deformation induced by self-desiccation [8-9]. The autogenous shrinkage of geopolymers is generally considered to be more severe than that of OPC, which can lead to uneven stress and deformation, resulting in the development of harmful cracks [10-11]. The ingress of aggressive ions through these cracks can not only impair the integrity of geopolymer, but also cause corrosion of internal steel reinforcement, reducing the durability of geopolymer concrete structures. Therefore, effective measures are required to mitigate the early-age deformation of geopolymers.

The addition of organic admixtures with hydrophobic modification capacity that can modulate the matrix wettability to alter pore pressure and water retention capacity may be a promising approach to mitigate the early-age shrinkage of geopolymers. Most researchers believe that the main driving force for autogenous shrinkage is pore pressure [11-13]. Sodium-based geopolymers have abundant microporous structures, and the size of pores in them is mainly in the range of 10–50 nm [14]. The continuous geopolymerization leads to a change of water content in pores from saturated to unsaturated state, i.e., the so-called self-desiccation effect. The meniscus of water columns located in the narrow pores generates greater pore pressure, which further promotes the early-age shrinkage [10,15]. It was found that the addition of organic admixtures can reduce the water loss and improve the hydrophobicity of pore walls, which effectively reduced the capillary pressure and increased the internal relative humidity, thereby alleviating the autogenous shrinkage by about 70% for alkali-activated materials [16]. Rath et al. [17] investigated the effect of organic rubber latex on the pore structure and capillary suction of geopolymer concrete and found that the addition of organic rubber latex can effectively decrease the early-age shrinkage of geopolymers. Huang et al. [18] reported that the use of edible oil can reduce the surface tension of concrete and make its internal structure denser, thereby effectively reducing the autogenous shrinkage of concrete by 68% without obvious strength loss. In addition, different from other frequently-used measurements for mitigating the shrinkage by adding internal curing admixtures [19-20] or shrinkage-reducing admixtures [11,21-22], modifying the wettability through organic admixtures can also enable the geopolymer with water repellence and corrosion resistance performance [23-26]. As hydrophobization can significantly reduce the capillary

force in the porous medium, the moisture and water carrying corrosive ions cannot easily penetrate. Thus, it is of great engineering and economic interests to mitigate the early-age shrinkage of geopolymers by means of hydrophobic modification.

Available organic admixtures can be divided into two types, including macromolecular polymers and micromolecular monomers. Macromolecular polymers tend to aggregate or attach to the pore wall or graft on the gel skeleton through active end groups, which sharply reduces the adsorption performance of the matrix to moisture. Silanes [25,27], siloxanes [26-27], organic emulsions and copolymers [28-30] have been proven to be hybridized with cementitious materials to alter their wettability, pore structure and deformation. Polydimethylsiloxane (PDMS) is a silicone polymer with superior chemical stability, water repellence and high adhesion. Cementitious materials containing PDMS have stable and durable hydrophobicity, strong corrosion resistance, as well as anti-icing and de-icing performance [26,31-33]. The authors' previous studies [23,34] indicated the modification of MKG by PDMS to achieve low water absorption capability, strong hydrophobicity and uniform microstructure. In contrast, micromolecular monomers can couple to inorganic matrix by participating in hydration or polymerization reactions, thereby forming a homogeneous and hydrophobic microstructure [35-36]. Sodium methylsilicate (SMS), as an organosilicate, can be hydrolysed in alkaline solution and produce monomers or oligomers with alkylated silicate structures and thus can participate in the geopolymerization to form modified geopolymers [37]. It can not only provide alkylated silicon units, but also serve as a component of alkaline activators to promote the dissolution of precursor and ensure the strength development of reaction products, because its aqueous solution exhibits strong alkalinity [38]. Alkali-activated slag containing methylsilicate had a dense microstructure, low water absorption and chloride permeability, because the hydrophobic group ($-CH_3$) from methylsilicate was grafted onto the gel chemical structure through condensation reaction [24]. SMS can also be used to prepare hydrophobic de-icing salts for concrete and inhibit the capillary adsorption properties of silt [39-40]. Although these organic admixtures with hydrophobic modification capacity have the potential to mitigate the early-age shrinkage of geopolymers, there is a lack of systematic study and analysis on their effects and mechanisms, which is of great significance to prevent the early-age cracking and increase the engineering benefits.

In this study, for the first time, the feasibility of PDMS and SMS as hydrophobic modifier to mitigate the early-age deformation of MKG paste was investigated. The autogenous shrinkage and

chemical expansion of MKG paste with various PDMS and SMS dosages during the first 7 days after casting were measured. Afterwards, a series of tests were conducted to characterise the pore structure, wettability, moisture/water adsorption capacity, and internal moisture distribution and transfer tendency of MKG paste using different techniques including mercury intrusion porosimetry (MIP) and low field ^{1}H nuclear magnetic resonance (LF-NMR) to estimate the effects of PDMS and SMS on the hydrophobic modification of MKG paste, which plays a critical role in moisture transport and early-age volume change. Based on the obtained experimental data, the underlying mechanisms of organic admixtures on mitigating early-age shrinkage of MKG paste were analysed and discussed in depth. This study lays the foundation for the engineering application of hydrophobized geopolymers with low early-age shrinkage, which are more promising as repair materials or protective coatings for infrastructures in high humidity or marine environments.

2. Experimental program

2.1 Raw materials

Metamax metakaolin (MK) obtained from BASF SE was used as precursor. Its chemical composition characterised using X-ray fluorescence as well as particle size distribution characterised using a Mastersizer 2000 laser particle size analyser and scanning electron microscope (SEM) image are presented in **Table 1** and **Fig. 1**, respectively. The volume-based average diameter of MK was 5.91 μm. The alkaline activator (AA) was a mixed solution of sodium silicate solution (SS, pH=10.4, SiO_2=26.0 wt.%, Na_2O=8.2 wt.%) and sodium hydroxide pellets (SH, purity: ⩾96%).

Table 1 Chemical composition of metakaolin (MK) (wt.%).

SiO_2	Al_2O_3	TiO_2	CaO	Fe_2O_3	Na_2O	K_2O	MgO	P_2O_5	Other
54.25	42.45	1.87	0.07	0.48	0.29	0.15	0.14	0.09	0.21

The used organic admixtures (i.e., PDMS and SMS) were both colourless and transparent liquids. PDMS was an oily siloxane with viscosity of 50 cst (Warwick Ruike Chemical Co., Ltd., China), while SMS was an aqueous liquid with a solid content of 30% and an alkalinity pH of 13.3 (Shanghai yuanye Bio-Technology Co., Ltd., China). **Fig. 2** displays their Fourier transform infrared (FTIR) spectra and chemical formula. Vibrations associated with methyl groups were detected, indicating the feasibility of hydrophobic modification by organic admixtures. The intense absorption peaks at 2959 cm^{-1}, 2903 cm^{-1}, and 1459 cm^{-1} originated from asymmetric/symmetric stretching and deformation vibrations of C−H bonds [41-42]. The symmetric bending of Si–CH_3 bonds appeared at wavelength

of 1262 cm^{-1} and 789 cm^{-1} [42].

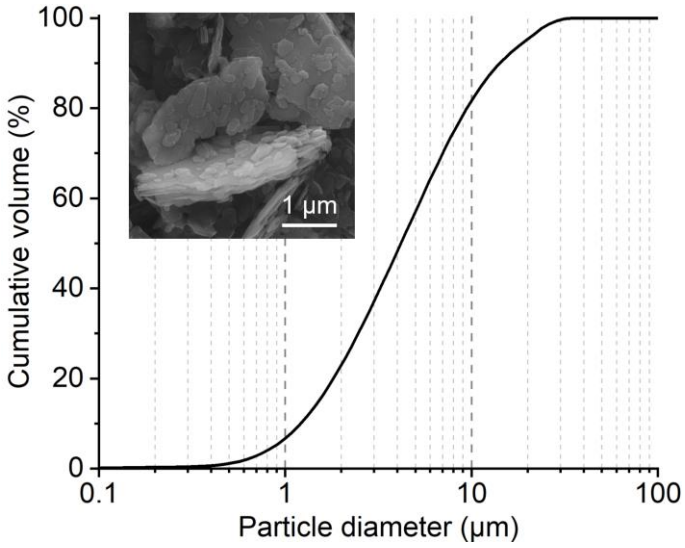

Fig. 1. Particle size distribution and morphology of MK.

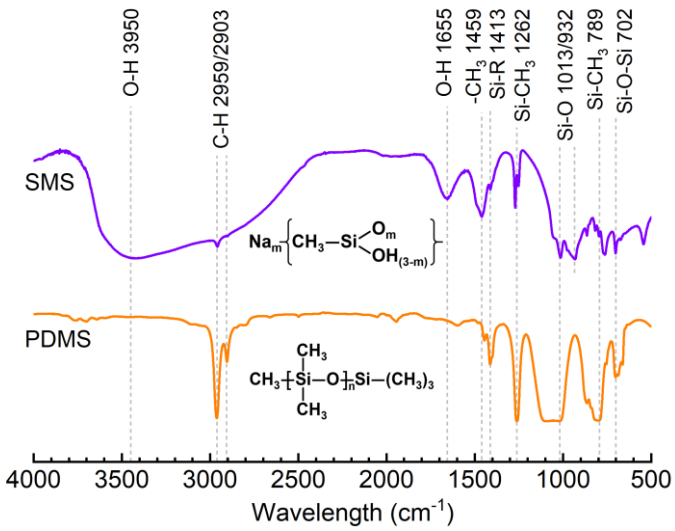

Fig. 2. FTIR spectra and chemical formula of polydimethylsiloxane (PDMS) and sodium methylsilicate (SMS).

2.2 Mix proportions

Table 2 presents the mix proportions of MKG pastes studied here based on a previous study [34], aiming to explore the effects of PDMS and SMS content. MKG paste without PDMS and SMS (i.e., G0) was considered as the reference mixture. Hydrophobized MKG pastes containing PDMS at a *m*(PDMS)/*m*(MK) ratio of 1% and 5% were denoted as GP1 and GP5, and hydrophobized MKG pastes containing SMS at a *n*(Na_2O in SMS)/[*n*(Na_2O in AA)+*n*(Na_2O in SMS)] ratio of 10% and 20% were denoted as GS10 and GS20, respectively. The SMS ratio here was referred to the molar ratio of Na_2O in SMS to that in alkaline activator and SMS. The total Na_2O content in MKG mixture was

0.0086 mol/(1g MK), and the molar ratio of the three main elements (Si, Al, and Na) was 1.85:0.95:1. The total water content in MKG mixture was 45 wt.%.

Table 2 Mix proportions of MKG pastes.

Specimen designation	MK (g)	SS (g)	SH (g)	PDMS (g)	m(PDMS)/m(MK) (%)	SMS (g)	n(Na_2O in SMS)/[n(Na_2O in AA)+n(Na_2O in SMS)] (%)	Water (g)
G0	100	160.0	17.3	\	\	\	\	35.4
GP1	100	160.0	17.3	1	1	\	\	36.0
GP5	100	160.0	17.3	5	5	\	\	39.5
GS10	100	140.2	15.9	\	\	33	10	26.8
GS20	100	120.5	14.6	\	\	66	20	18.1

2.3 Specimen preparation

During the mixing, MK, alkaline activator, SMS (only for GS10 and GS20) and water were added into a container and stirred for 6–10 min. For GP1 and GP5 specimens, PDMS was first added to the alkaline solution, and the mixed liquid was stirred at a high speed of 1,200 r/min for 2 minutes to ensure that PDMS is emulsified and well dispersed. The fresh paste was then poured into moulds and sealed cured under ambient conditions (25±2 °C) until the testing ages.

2.4 Testing methods

2.4.1 Chemical deformation test

Chemical deformation was measured as per ASTM C1608-12 [43], as illustrated in **Fig. 3**. After mixing, 50 mL of the fresh MKG paste was poured into a rigid plastic jar, and sodium hydroxide solution with pH of 12.5 was then slowly added to the jar to full. The alkalinity of the sodium hydroxide solution was similar to that of the fresh paste (pH=12–13), which could prevent the paste from being diluted. A rubber stopper inserted with a graduated capillary tube was adopted to cover the jar, and some paraffin oil was dropped on the alkali solution surface in the capillary tube to prevent water evaporation. To reduce the effect of temperature change, the jars containing pastes were placed in a polystyrene box added with water at a temperature of 25±2 °C. The chemical deformation data referring to the volume change of water in tube were obtained by taking pictures at regular intervals. To eliminate the effect of the device, data were read 1 hour after paste mixing, and this moment was defined as the origin of the test [44]. The chemical deformation denotes the volume change induced by each gram of pasty specimens and was continuously recorded for 7 days.

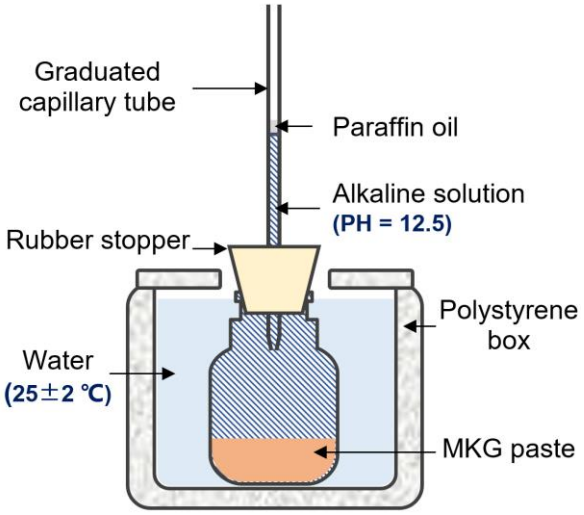

Fig. 3. Schematic illustration of chemical deformation measurement.

2.4.2 Autogenous deformation test

Autogenous deformation was measured according to ASTM C1698-09 standard [45] using a non-contact corrugated tube device shown in **Fig. 4**. The corrugated tube was 420±5 mm long and 29±0.5 mm outside diameter. It was made of flexible plastic to minimise the resistance to longitudinal expansion and contraction. The fresh MKG paste was poured into the tube to fill the entire tube which was then closed with a stopper. The eddy current displacement sensor was used to automatically collect the autogenous deformation data of the first 7 days of geopolymerization to further improve the test accuracy. During the entire testing period, paste specimens and instruments were kept in a controlled environment room at temperature of 25±2 °C.

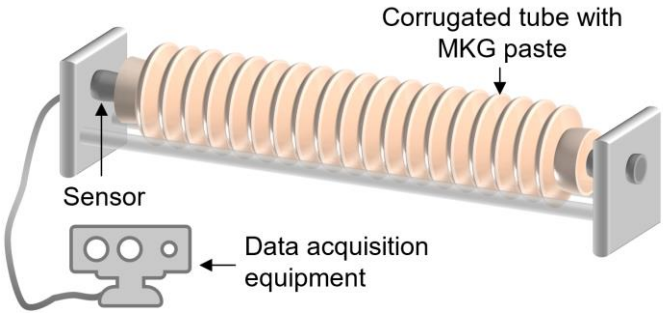

Fig. 4. Test setup for measuring autogenous deformation.

2.4.3 Mercury intrusion porosimetry

The pore structure of all MKG pastes in terms of size distribution, threshold diameter and intrusion porosity was characterised using MIP (AutoPore IV9500 automatic mercury intrusion meter) that allows a range of pressures from 0 to 60,000 psia, corresponding to pore diameters of 3 nm−360 μm. Specimens cured for 7 days were processed into particles of about 2 mm in diameter and dried at 65 ℃

for 48 hours before testing.

2.4.4 Water contact angle test

The water contact angle tests were carried out using a DropMeter A-100P contact angle measuring instrument (Haishu Maishi Testing Technology Co., Ltd., China) to characterise the integral wettability. The water contact angles of three types of the matrix surfaces were measured, i.e., rough fracture surfaces cut by cutting machine, fracture surface polished by 400-, 800-, 1200-, and 2000-mesh sandpapers, and surface scratched with a knife. MKG pastes cured for 7 days were wiped and dried at 40 ℃ for 8 hours before the test.

2.4.5 Moisture adsorption test

The moisture (i.e., water vapor) adsorption capacity was tested on Ø55×5–7 mm disc specimens weighing approximately 30 g. MKG pastes cured for 7 days were dried at 40 ℃ to reduce the moisture content by about 25 wt.%. A drying temperature of 40 ℃ has been reported as appropriate for minimising the microstructural alteration of cementitious materials [46-47]. The sides of the discs were sealed with plastic tape to maintain one-dimensional moisture transport from the two bottom surfaces. During the test, the paste specimen was erected in a box with relative humidity of 90±5%. The water vapor would not condense into water droplets at such relative humidity, and thus the moisture diffusion rate could be determined rapidly.

2.4.6 Water adsorption test

The water adsorption capacity was tested on cubic specimens with 50-mm sides after curing for 7 days in accordance with ASTM C642-13 [48]. Before the test, MKG pastes were wiped and then dried at 40 ℃ to evaporate approximately 25 wt.% of water with no visible cracks. The specimens were sealed with epoxy resin on all except the side in direct contact with water to ensure one-dimensional water flow. Subsequently, they were immersed in water with a depth of about 3 mm, and the mass gain was measured periodically.

2.4.7 Low field ^{1}H nuclear magnetic resonance

Moisture distribution and transfer in MKG pastes were characterised using a LF-NMR imaging system, MesoMR23-060H-I (Suzhou Niumai Analytical Instrument Co., Ltd., China). After mixing, 10 g of the prepared paste was transferred by a pipette into a threaded glass bottle, which was then sealed to prevent water exchange. The glass bottle containing the paste was then cured at room temperature of 25±2 °C. MKG pastes cured for 6 hours, 1 day, and 7 days were put into the test

chamber for in-situ testing, and the transverse relaxation time (T_2) distribution spectrum was further obtained. LF-NMR can detect T_2 based on ^1H intrinsic relaxation behaviour of water in the specimens, which reveal the exchange process of water protons due to diffusional interchange of water protons between free water and bound water molecular [49]. The signal scanning adopted CPMG sequence, and the main frequency and number of sampling points were set as 23 MHz and 540018, respectively.

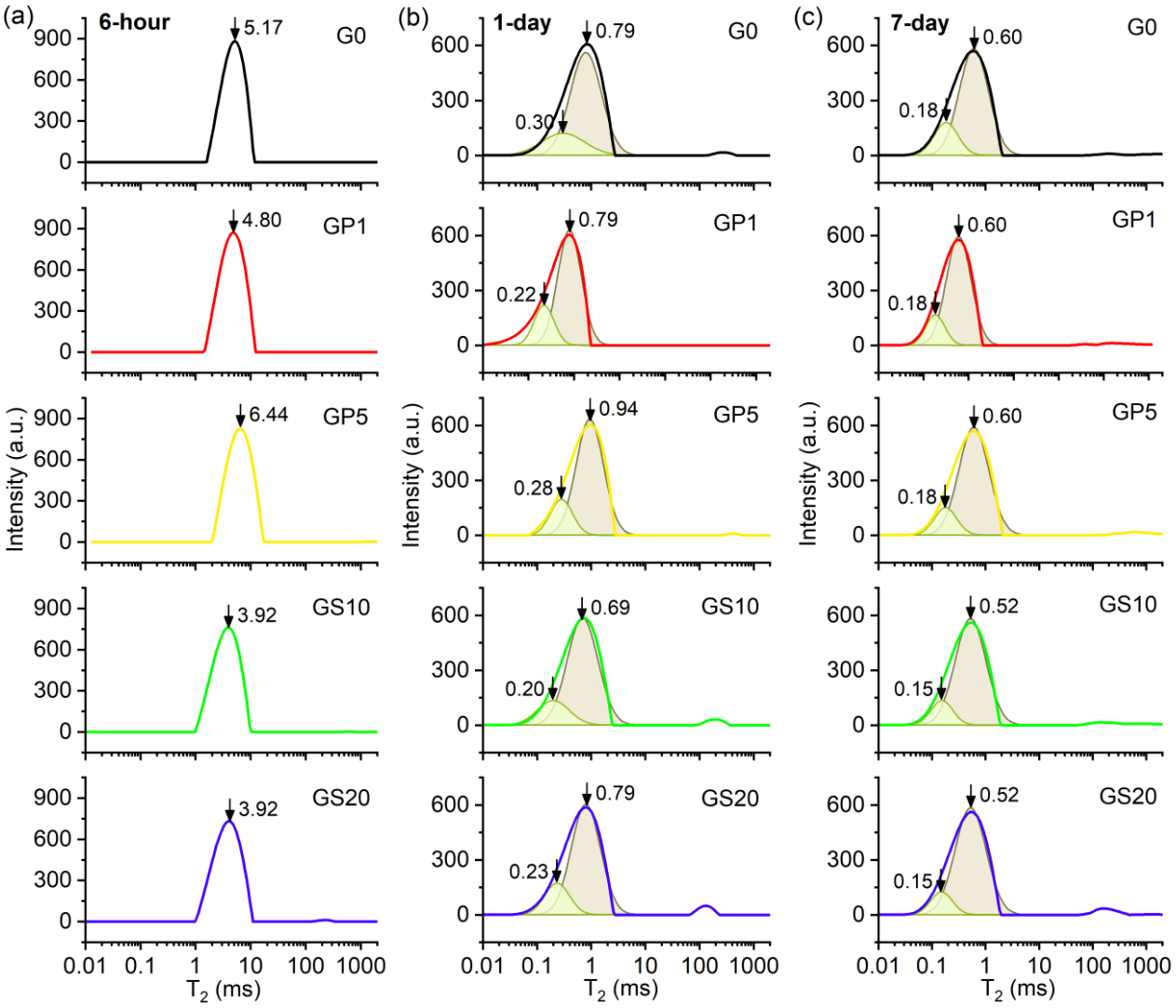

Fig. 5. T_2 intensity and distribution of MKG mixtures during geopolymerization at (a) 6 hours, (b) 1 day, and (c) 7 days of curing (single peaks with a fill colour denote the deconvolution results fitted by Gaussian curves).

Fig. 5 displays the T_2 intensity and distribution of MKG pastes at 6 hours, 1 day, and 7 days. Signals with close T_2 values tend to result in overlapping intensity peaks (**Fig. 5**b and c). As per Ref. [50], the main peaks (T_2<1 ms) of MKG cured for 1 day and 7 days were deconvolved into two Gaussian curves using Origin software to obtain separated T_2 signals. The deconvolution process

follows two principles: (1) the T_2 value corresponding to the peak of a Gaussian curves is equal to the T_2 value corresponding to the peak of the original main-peak curve; (2) the correlation coefficient exceeds 0.98.

3. Experimental results

3.1 Chemical deformation

Fig. 6 illustrates the chemical deformation of MKG pastes with and without organic admixtures, which represents the volume change due to the difference in average density between reaction products and fresh aluminosilicate paste [6-7]. As seen in **Fig. 6**, the chemical deformation of MKG pastes can be divided into three main stages. After a short shrinkage (0–4 hours), all MKG pastes sequentially experience a rapid expansion in the second stage (4 hours–4 days) and a slow shrinkage again in the final stage (after 4 days). This is consistent with the finding reported by Li et al. [51].

Compared to the reference MKG paste, the 7-day chemical expansion of hydrophobized MKG pastes with the addition of PDMS and SMS is obviously reduced. This implies that these organic admixtures can affect the geopolymerization progress and the structure of N-A-S-H gels. The chemical shrinkage in the first 4 hours can be mainly ascribed to the dissolution of MK and the formation of aluminosilicate oligomers [52]. The initial chemical shrinkage of hydrophobized MKG pastes is faster and lasts longer, as PDMS disperses the solid precursor and SMS increases the alkalinity of the system. The chemical expansion in the first 4 days can be mainly attributed to the formation of aluminium-rich zeolite products which dominates this geopolymerization stage [51,53]. After 4 days of curing, the reorganization and polymerization of aluminium-rich products and silicate oligomers dominate the reaction, forming amorphous silica-rich gels with higher density, so that all MKG pastes experience chemical shrinkage [54]. The addition of SMS can effectively slow down the chemical expansion rate of MKG paste, indicating that it may inhibit the formation of aluminium-rich gels or promote the polymerization of silica-rich gels. The fluctuations of chemical deformation at 1.5–4 days for GS10 and GS20 also support such inference. During this period, the organosilicon molecules from SMS are involved in the reaction, and the aluminium-rich and silica-rich products compete to dominate the reaction process.

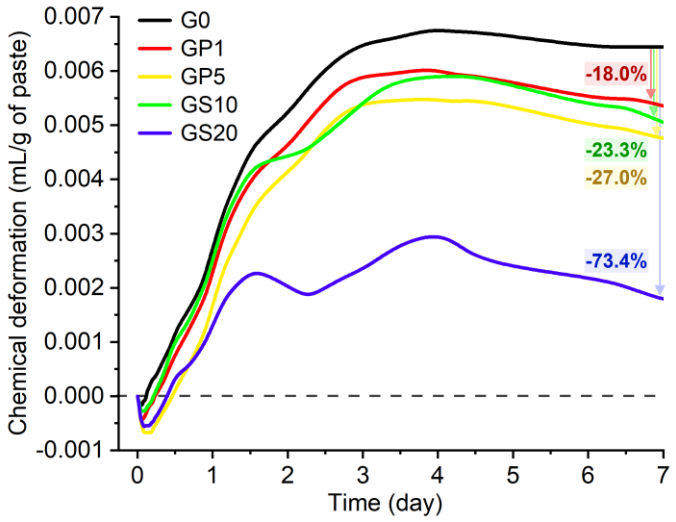

Fig. 6. Chemical deformation of MKG pastes during the first 7 days.

3.2 Autogenous deformation

Fig. 7 shows the autogenous deformation development of MKG pastes, which is one of the most intuitive features to describe the early-age volume stability. The results indicate that the reference MKG paste maintains the highest autogenous shrinkage consistently, and its 7-day autogenous shrinkage reaches 3,550 μm/m, which is slightly higher than that of OPC (generally considered to be less than 2,500 μm/m within 24 hours) [55-57]. This can be ascribed to the self-desiccation resulting from the evolution of the gel and pore structures [58]. The inconsistency in the development of autogenous and chemical deformations also suggest the dominant effect of self-desiccation on the early-age deformation. It can be noted that both PDMS and SMS can effectively inhibit the autogenous shrinkage of MKG pastes, which is of great significance to suppress the early-age cracking and improve the durability of MKG [59].

According to **Fig. 7**b, the autogenous shrinkage rate is the highest within the first day for all MKG pastes, during which the fresh paste undergoes drastic self-desiccation and gradually hardens to form a porous gel structure [60]. The autogenous shrinkage rate of GP0 reaches the maximum value at 15.4 hours, and the addition of PDMS and SMS delays this moment by 0.7–4.5 hours. Moreover, MKG pastes containing PDMS exhibit slight and slow expansion in the first 12 hours and after 2 days of curing, which was also reported in other studies on sodium-based geopolymers [61-62]. The mitigation of autogenous shrinkage of the MKG paste by the organic admixtures can be explained by the modification of matrix wettability and microstructure, which will be analysed in the following sections.

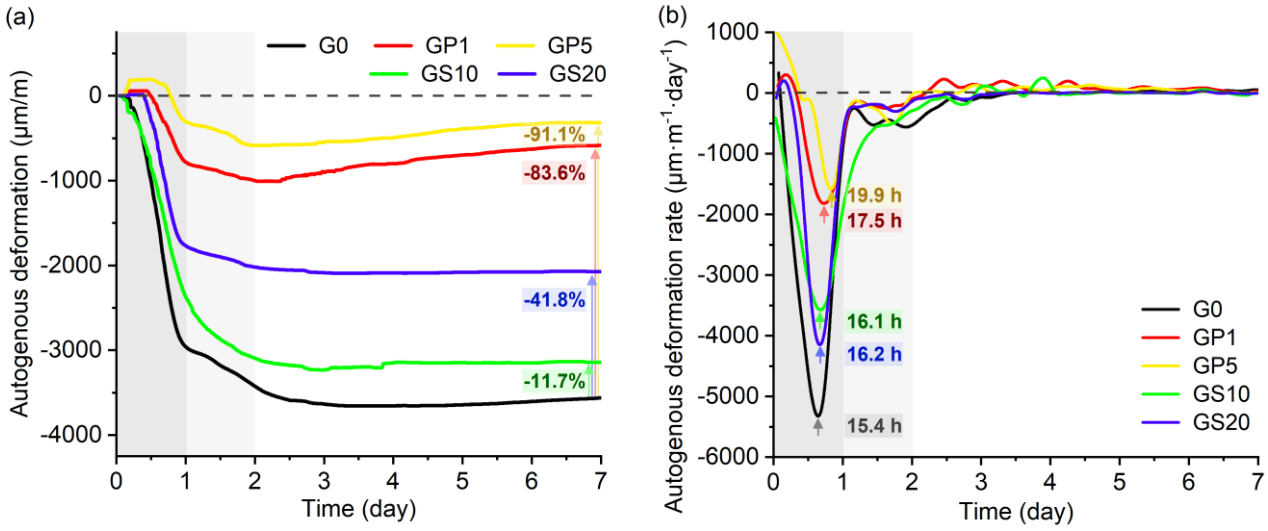

Fig. 7. Development of autogenous deformation of MKG pastes during the first 7 days: (a) autogenous deformation, and (b) autogenous deformation rate (i.e., first derivative of autogenous deformation curves).

3.3 Pore structure characteristics

Fig. 8 displays the pore structure characteristics of 7-day cured MKG pastes measured by MIP, which can be used to quantify the microstructural evolution and evaluate the associated properties. As seen in **Fig. 8**a, the pores are concentrated at 10–50 nm in diameter. These pores are denoted as medium capillary pores, which are closely related to the capillary tension magnification established at the meniscus. According to the study of Mehta et al. [63], other pores with diameters of <10 nm, 50–10,000 nm, and >10,000 nm are referred to as gel pores, large capillary pores, and air voids, respectively. **Fig. 8**c and d show the total intrusion porosity and porosity for those in different diameter ranges. The total porosity is similar in all MKG pastes, while the addition of the organic admixtures can reduce the pore size (**Fig. 8**b) and promote the transformation of medium capillary pores into smaller gel pores. The gel porosity of hydrophobized MKG pastes goes up compared to that of G0, implying that the organic admixtures may lead to a more pronounced self-desiccation in modified MKG pastes as the internal capillary force is highly correlated with small pores [19].

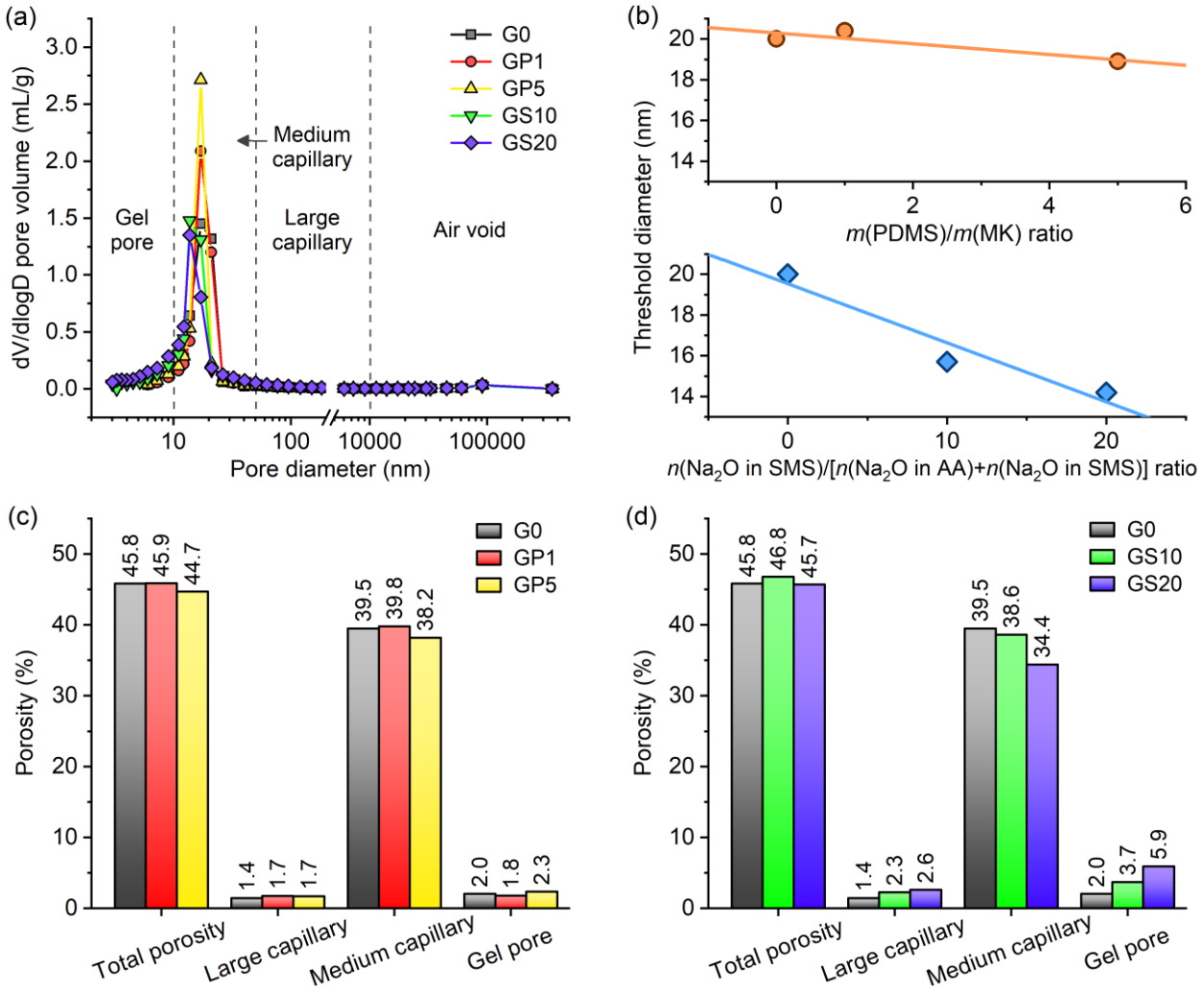

Fig. 8. Pore structure characteristics of 7-day MKG pastes: (a) pore size distribution, (b) threshold diameter, as well as total intrusion porosity and porosity for those in different diameter ranges of specimens with (c) PDMS and (d) SMS.

3.4 Wettability

Fig. 9 shows the water contact angle results for the dried MKG matrix, revealing the intrinsic wettability change induced by the addition of organic admixtures. MKG paste can be hydrophobically modified by PDMS and SMS with water contact angles of approximately 130° and 140°, respectively. Their hydrophobicity is robust and long-lasting, which would not be impaired by cutting, crushing, mechanical grinding, or scratching. The water contact angle reflects the tension balance between the three-phase interface and is closely related to the free energy and morphology of the contact surface [64]. The hydrophobic chemical groups introduced through the addition of PDMS or SMS can be tightly attached to the gel in the form of adsorption, entanglement, or grafting. The reduction of the surface energy caused by the chemical composition change leads to the hydrophobic modification [23,37]. The wettability change not only affects the autogenous deformation induced by self-

desiccation but also enables MKG pastes with promising water repellence.

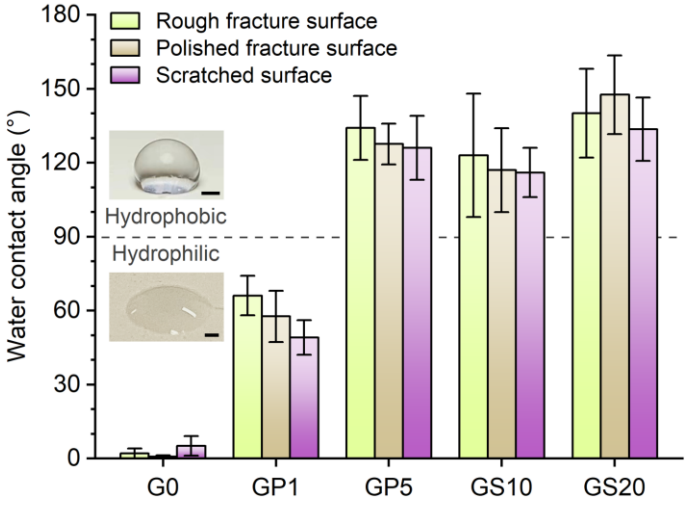

Fig. 9. Water contact angle results of the dried MKG matrix (rough fracture surface, polished fracture surface, and scratched surface; scale bar:1 mm).

3.5 Moisture/water adsorption capacity

Moisture and water adsorption behaviour reveals the capacity of the MKG matrix to attract and bind gaseous and liquid water and can also be used to evaluate the waterproof performance. **Fig. 10**a displays the time-evolution of the moisture absorptivity. The slope of the fitted line represents the moisture absorptivity rate, which decreases by 33.3%–62.5% with the addition of PDMS or SMS. In addition, as seen in **Fig. 10**b, the water absorptivity rate and the final absorptivity of hydrophobized MKG pastes also show a drastic drop. GP5 exhibits the multi-stage water adsorption behaviour with a low-absorptivity stage during the first 12 hours, which is closely related to its low moisture absorptivity during this period of time. The hydrophobic PDMS layer that physically adsorbs to the capillary pores of MKG can inhibit water adsorption but cannot prevent water vapor diffusion. Thus, GP5 still presents water absorption capacity when the PDMS layer is covered by condensed water [34]. In contrast, GS10 and GS20 keep extremely low one-dimensional adsorption rate throughout the test period of over 100 days, and their final absorptivity sharply drops by over 80% and 95%, respectively. This can be explained by the fact that SMS molecules grafted directly onto the gels change the chemical composition of GS10 and GS20. The moisture and water adsorption capacity of the hydrophobized MKG paste is significantly weakened due to the sharp reduction in surface tension and capillary suction, and thus water is more difficult to adsorb and remains on their pore walls [65]. Furthermore, these modified MKG pastes exhibit excellent water repellence and resistance to

permeation because of the hybridization of organic admixtures, which is significant for improving the durability and corrosion resistance properties.

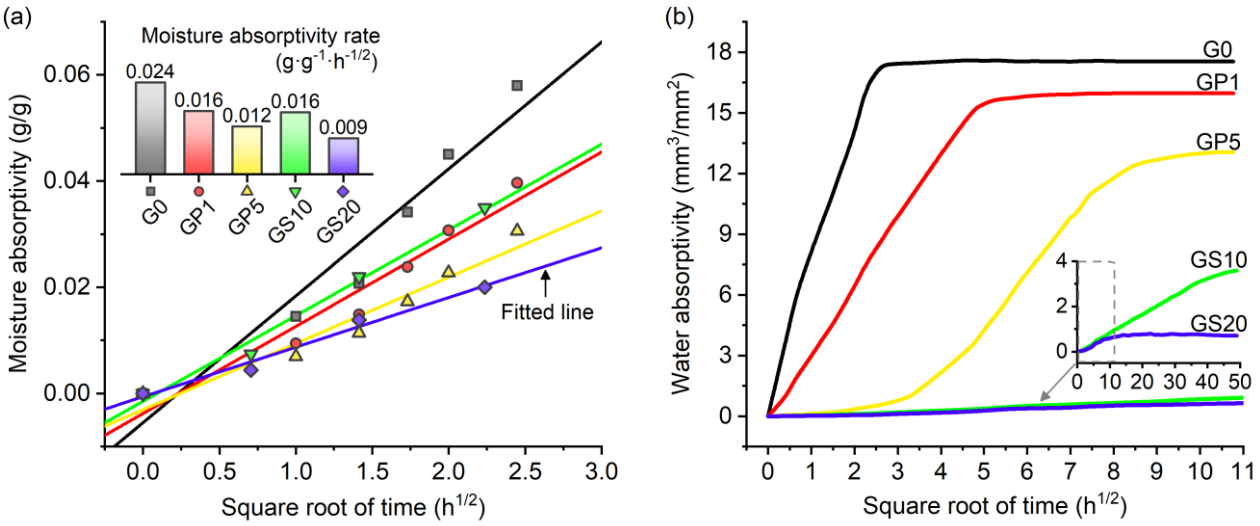

Fig. 10. Time-evolution of (a) moisture and (b) water absorptivity during the tests (the inset of (a) representing the moisture absorptivity rate that is the slope of the fitted line for moisture absorptivity-square root of time; the inset of (b) is time-evolution of water absorptivity for GS10 and GS20 over 100 days).

3.6 Internal moisture distribution

As seen in **Fig. 5**, the internal moisture distribution can be investigated using T_2 signals obtained through LF-NMR to analyse the capillary stress characteristics of MKG paste [66]. Moisture in cementitious materials is considered to be bound in pores in the form of inter-gel water, capillary water and free water [49,67]. According to the relevant studies [68-69], T_2 peaks represent the moisture bound to the matrix in different binding states and the signal amplitude describes the pore fluid content.

Fig. 11 displays T_2 and its corresponding internal moisture distribution in MKG pastes. As seen in **Fig. 11**a, T_2 curves of the 6-hour cured MKG paste shows a main peak representing free water at around 5 ms. Water as a medium for dissolving silicon-oxygen and aluminium-oxygen oligomers has a high degree of freedom at this stage [53,70]. The T_2 value and intensity of 1-day cured MKG pastes are significantly reduced (**Fig. 11**b). This suggests that aluminosilicate precursors are converted into a strong gel skeleton through geopolymerization, so that the freedom of water is limited and the water is considered as capillary water. The results of Gaussian function deconvolution also reveal the presence of inter-gel water, which is adsorbed tightly to gel pores (**Fig. 5**b). These gel pores and

medium capillary pores are defined as mesopores (2.5−50 nm) by the International Union of Pure and Applied Chemistry (IUPAC), and their transfer and loss have a significant effect on the early-age deformation [6,71]. As seen in **Fig. 11**c, the main T_2 peak of 7-day cured MKG pastes shift slightly negatively, indicating that the degree of freedom of water drops and the water-binding capacity of the matrix goes up as the reaction proceeds [72]. Moreover, some small dispersion peaks representing highly free water appear at T_2 of >100 ms due to the increased interconnected micron-scale voids or defects resulting from skeleton development. The gain or loss of these free water has little effect on the volume change [73-74].

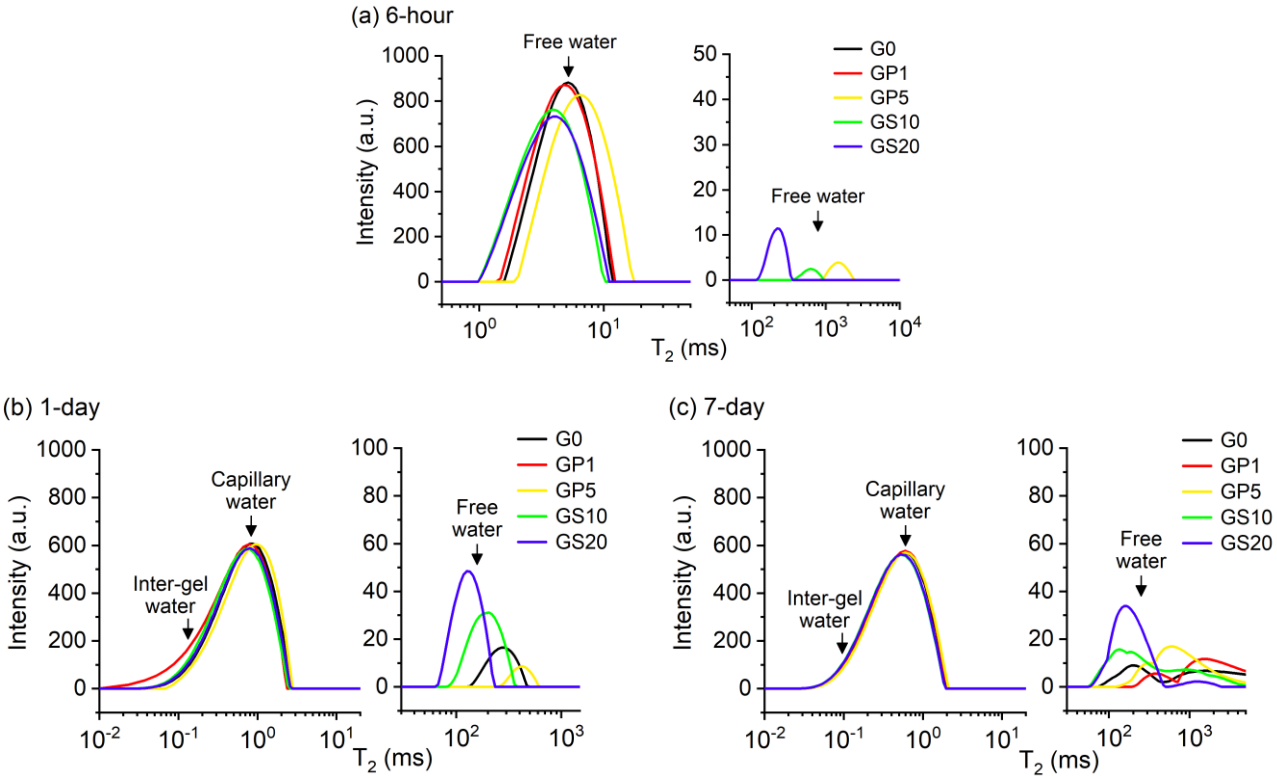

Fig. 11. T_2 and the corresponding internal moisture distribution in MKG pastes cured for (a) 6 hours, (b) 1 day, and (c) 7 days.

Fig. 12 presents the proportion of moisture in different binding states obtained by integrating Gaussian curves. The initial water cannot fill all newly generated gel pores and capillary pores during geopolymerization, as the chemical deformation results indicate that the gel skeleton expands. Thus, the self-desiccation behaviour leads to moisture redistribution and unsaturated MKG pastes. As shown in **Fig. 12**a and b, during the first day of the reaction, the addition of PDMS reduces the growth rate of free water (T_2>100). It was reported that MKG paste exhibits significant dehydration during curing and free water can condense on the surface of specimens [75]. Oily liquid PDMS is more

readily adsorbed on the surface of MK than dispersed in alkaline solution and thus may inhibit the dissolution and early reaction of the precursor. In contrast, MKG pastes with SMS contain more free water because SMS with highly alkalinity promotes drainage while participating and enhancing the reaction progress. As seen in **Fig. 12**c, the inter-gel water in the 7-day cured MKG pastes has stronger binding capacity but lower proportion. The effect of organic admixtures on moisture distribution can be attributed to the moisture transfer induced by wettability modification. It is also the main reason for the reduced early-age shrinkage, which will be further discussed in Section 4.

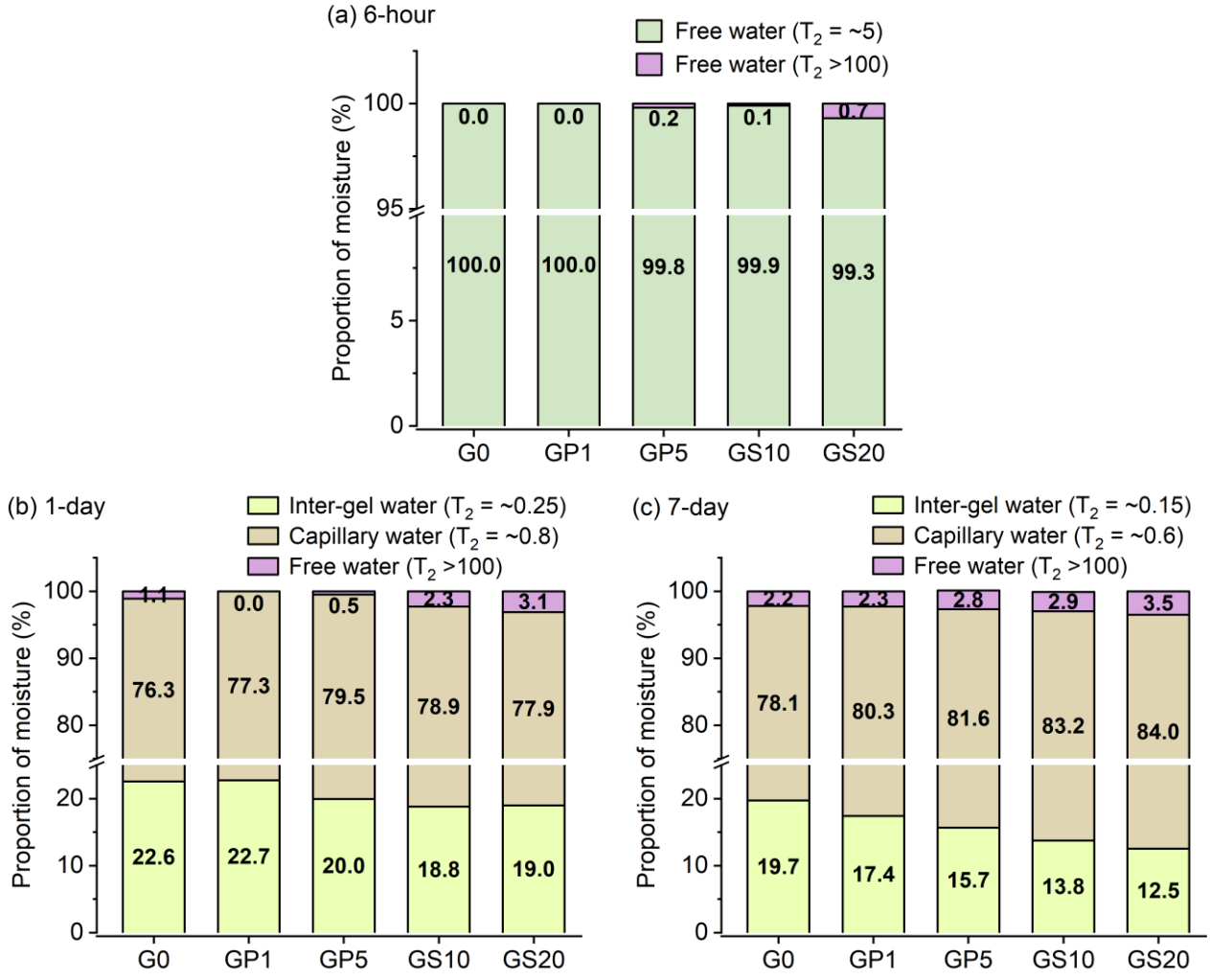

Fig. 12. Proportion of moisture in different binding states for MKG pastes cured for (a) 6 hours, (b) 1 day, and (c) 7 days.

4. Discussion

In order to discuss the general effect and underlying mechanism of organic admixture addition on autogenous shrinkage of MKG paste, the internal capillary stress characteristics in MKG paste are further analysed based on the experimental findings above. According to Young-Laplace law, under ideal conditions (ignoring gravity, adhesion, and air pressure), the stress acting on water in

unsaturated pores (σ) relates to the surface tension of the pore water (γ), the water/pore wall contact angle (θ), and the pore radius (r) as follows [76]:

$$\sigma = -\frac{2\gamma cos\theta}{r} \quad (1)$$

Fig. 13 displays the schematic diagrams of moisture transfer trend and possible distribution states in pores of different size in MKG pastes. As seen in **Fig. 13**a, the contact angle θ_r of water and the pore wall for the reference MKG paste is less than 90° due to its hydrophilic matrix, so that water tends to spread in pores rather than agglomerate [77]. The stress on the meniscus in smaller pores (such as gel pores and medium capillary pores) $\sigma_{s\text{-}r}$ is higher than that in the larger pores (such as large capillary pores) $\sigma_{l\text{-}r}$. Therefore, as the pore structure is formed during geopolymerization, water tends to be transferred and stored into smaller pores in a more stable manner. However, since the water in pores in the real state is also affected by gravity, matrix adhesion, and air pressure, it can also be adsorbed in larger pores before filling gel pores and small capillary pores to saturation. In summary, a possible water distribution state as illustrated in **Fig. 13**c will be formed in the reference MGK paste in the state of external force balance.

In contrast, the direction of the meniscus and stress of water in the hydrophobized MKG paste are opposite to those in the reference MKG due to the wettability modification. As demonstrated in **Fig. 13**b, water tends to be transported and collected to relatively large capillary pores rather than narrow gel pores. The hydrophobic layer of adsorbed or grafted methyl groups from PDMS or SMS reduces the surface energy of the pore wall, making the water/pore wall contact angle θ_h of the hydrophobized MKG paste larger than 90°. Owing to the stress difference, water in smaller pores is squeezed into larger capillary pores, leading to the possible water distribution state shown in **Fig. 13**d.

According to Newton's third law of motion, the MKG skeleton is also subjected to a stress σ_m induced by the surface tension of the liquid-gas meniscus, which is generally considered to be a key cause of early-age shrinkage of cementitious materials [6]. The greater the mean stress of the liquid-gas meniscus inside the matrix, the greater the shrinkage caused by self-desiccation. During the self-desiccation process, the adsorbed water in both gel and capillary pores generates more scattered liquid columns and liquid-vapor meniscus due to redistribution, which leads to a continuous increasing stress on the matrix. These stresses with different directions and magnitudes tend to compress the matrix further, and thus cause shrinkage. MKG pastes exhibit relatively fast self-desiccation and ear-

age shrinking during the first two days of geopolymerization due to rapid expansion of the gel matrix (**Fig. 6**) and dramatic changes in moisture distribution (**Fig. 12**). As for hydrophobized MKG pastes, water is more likely to be stabilized in pores with larger size due to the hydrophobic matrix, resulting in relatively lower internal stress $\sigma_{m\text{-}h}$. In addition, the aggregation-preferred moisture transport tendency leads to less dispersed water column and liquid-gas meniscus in the matrix, and thus the hydrophobized MKG paste is less prone to deformation compared to the reference MKG paste. Therefore, the organic admixtures have a significant mitigation effect on the early-age shrinkage of MKG paste. The autogenous shrinkage of MKG mainly depends on the matrix wettability, internal moisture distribution and stress characteristics but is not so associated with the water loss, which is consistent with the findings by other studies [78-80].

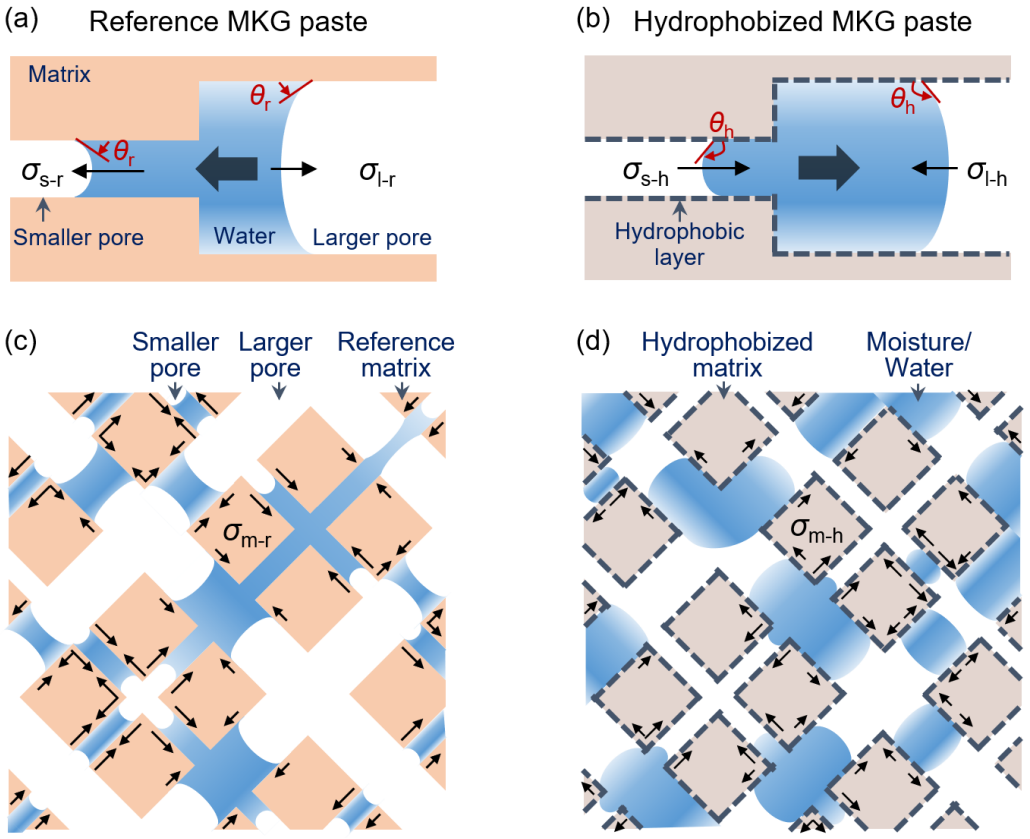

Fig. 13. Schematic diagrams of moisture transfer trend and possible distribution states in pores of different size in MKG pastes: (a) water in pores of reference MKG pastes tending to transfer from larger pores to smaller pores, (b) water in pores of hydrophobized MKG pastes tending to transfer from smaller pores to larger pores, as well as possible equilibrium water distribution during early-age geopolymerization in (c) reference and (d) hydrophobized MKGs (black arrows represent the stress σ_m on the matrix induced by the surface tension of the meniscus).

5. Conclusions

In this study, the feasibility of using organic admixtures (PDMS and SMS) as hydrophobic modifiers to mitigate the early-age shrinkage of MKG paste as well as underlying mechanisms are investigated by evaluating the porous structure, wettability, moisture/water adsorption capacity, and internal moisture distribution of MKG paste with and without these organic admixtures. Based on the experimental results and theoretical analysis, the following conclusions can be drawn:

- Chemical expansion and autogenous shrinkage of MKG pastes are significantly reduced by the addition of organic admixtures. When incorporating 5% PDMS (by MK mass) and 20% SMS (molar ratio of Na_2O in SMS to that in alkaline activator and SMS) into the mixture, the chemical expansion of MKG paste is reduced by 27.0% and 73.4%, and its autogenous shrinkage is decreased by 91.1% and 41.8%, respectively.
- The addition of PDMS or SMS promotes the transformation of medium capillary pores (10–50 nm) into smaller gel pores (<10 nm), which may lead to a more pronounced self-desiccation.
- MKG pastes are hydrophobically modified by PDMS and SMS that can be tightly attached to the matrix with water contact angles of approximately 130° and 140°, respectively. Therefore, the sharp reduction in surface tension and capillary suction leads to a decrease in the moisture and water adsorption capacity of the hydrophobized MKG paste by 33.3%–62.5% and 9.0%–95.9%, respectively. The enhanced water resistance also suggests that the adopted organic admixtures are beneficial to the durability of MKG paste.
- The internal moisture distribution and transfer tendency of unsaturated MKG pastes mainly depend on the matrix wettability. In contrast to the hydrophilic reference MKG paste, water in the hydrophobized MKG paste tends to be transported and stored into relatively larger capillary pores rather than narrow gel pores, and thus their inter-gel water proportion is reduced, and the capillary water proportion is increased.
- Hydrophobic modification by adding organic admixtures is an effective approach to mitigating the early-age autogenous shrinkage of MKG paste. The moisture/water in the hydrophobized MKG is more likely to accumulate in the larger pores, which leads to less dispersed liquid-vapor meniscus and lower internal stress induced by its surface tension, thereby contributing substantially to the mitigation of early-age shrinkage.

Acknowledgements

The authors greatly acknowledge the financial support from the National Natural Science Foundation of China (Nos. 51978608, 52171277 and 52101328) and Shanxi-Zheda Institute of Advanced Materials and Chemical Engineering (No. 2022SZ-TD006). The financial support provided by China Scholarship Council (CSC) to the first author is also gratefully acknowledged.

References

[1] B.C. McLellan, R.P. Williams, J. Lay, A. van Riessen, G.D. Corder, Costs and carbon emissions for geopolymer pastes in comparison to ordinary Portland cement, Journal of Cleaner Production 19(2011) 1080-1090.

[2] M. Amran, S. Debbarma, T. Ozbakkaloglu, Fly ash-based eco-friendly geopolymer concrete: a critical review of the long-term durability properties, Construction and Building Materials 270(2021) 121857.

[3] P. Cong, Y. Cheng, Advances in geopolymer materials: a comprehensive review, Journal of Traffic and Transportation Engineering (English Edition) 8(2021) 283-314.

[4] P. Zhang, K. Wang, Q. Li, J. Wang, Y. Ling, Fabrication and engineering properties of concretes based on geopolymers/alkali-activated binders - a review, Journal of Cleaner Production 258(2020) 120896.

[5] M. Lahoti, K.H. Tan, E. Yang, A critical review of geopolymer properties for structural fire-resistance applications, Construction and Building Materials 221(2019) 514-526.

[6] S. Tang, D. Huang, Z. He, A review of autogenous shrinkage models of concrete, Journal of Building Engineering 44(2021) 103412.

[7] M. Geiker, T. Knudsen, Chemical shrinkage of Portland cement pastes, Cement and Concrete Research 12(1982) 603-610.

[8] A.A. Melo Neto, M.A. Cincotto, W. Repette, Drying and autogenous shrinkage of pastes and mortars with activated slag cement, Cement and Concrete Research 38(2008) 565-574.

[9] T. Yang, H. Zhu, Z. Zhang, Influence of fly ash on the pore structure and shrinkage characteristics of metakaolin-based geopolymer pastes and mortars, Construction and Building Materials 153(2017) 284-293.

[10] N.K. Lee, J.G. Jang, H.K. Lee, Shrinkage characteristics of alkali-activated fly ash/slag paste and mortar at early ages, Cement and Concrete Composites 53(2014) 239-248.

[11] B. Zhang, H. Zhu, P. Feng, P. Zhang, A review on shrinkage-reducing methods and mechanisms

of alkali-activated/geopolymer systems: effects of chemical additives, Journal of Building Engineering 49(2022) 104056.

[12] P. Lura, O.M. Jensen, K. van Breugel, Autogenous shrinkage in high-performance cement paste: an evaluation of basic mechanisms, Cement and Concrete Research 33(2003) 223-232.

[13] Z. Li, X. Liang, Y. Chen, G. Ye, Effect of metakaolin on the autogenous shrinkage of alkali-activated slag-fly ash paste, Construction and Building Materials 278(2021) 122397.

[14] S. Chen, S. Ruan, Q. Zeng, Y. Liu, M. Zhang, Y. Tian, D. Yan, Pore structure of geopolymer materials and its correlations to engineering properties: a review, Construction and Building Materials 328(2022) 127064.

[15] H. Chen, M. Wyrzykowski, K. Scrivener, P. Lura, Prediction of self-desiccation in low water-to-cement ratio pastes based on pore structure evolution, Cement and Concrete Research 49(2013) 38-47.

[16] Z.Y. Qu, Q. Yu, Y.D. Ji, F. Gauvin, I.K. Voets, Mitigating shrinkage of alkali activated slag with biofilm, Cement and Concrete Research 138(2020) 106234.

[17] B. Rath, Effect of natural rubber latex on the shrinkage behavior and porosity of geopolymer concrete, Structural Concrete (2021) 1-12.

[18] J. Huang, J. Yan, K. Liu, B. Wei, C. Zou, Influence of cooking oil on the mitigation of autogenous shrinkage of alkali-activated slag concrete, Materials 13(2020) 4907.

[19] W. Tu, Y. Zhu, G. Fang, X. Wang, M. Zhang, Internal curing of alkali-activated fly ash-slag pastes using superabsorbent polymer, Cement and Concrete Research 116(2019) 179-190.

[20] C. Song, Y.C. Choi, S. Choi, Effect of internal curing by superabsorbent polymers - internal relative humidity and autogenous shrinkage of alkali-activated slag mortars, Construction and Building Materials 123(2016) 198-206.

[21] Y. Ling, K. Wang, C. Fu, Shrinkage behavior of fly ash based geopolymer pastes with and without shrinkage reducing admixture, Cement and Concrete Composites 98(2019) 74-82.

[22] Y. Yang, Z. Chen, W. Feng, Y. Nong, M. Yao, Y. Tang, Shrinkage compensation design and mechanism of geopolymer pastes, Construction and Building Materials 299(2021) 123916.

[23] S. Ruan, S. Chen, X. Zhu, Q. Zeng, Y. Liu, J. Lai, D. Yan, Matrix wettability and mechanical properties of geopolymer cement-polydimethylsiloxane (PDMS) hybrids, Cement and Concrete Composites 124(2021) 104268.

[24] X. Lv, Y. Qin, H. Liang, Y. Han, J. Li, Y. He, X. Cui, Potassium methyl silicate (CH_5SiO_3Na) assisted activation and modification of alkali-activated-slag-based drying powder coating for protecting cement concrete, Construction and Building Materials 326(2022) 126858.

[25] C. Zhang, S. Zhang, J. Yu, X. Kong, Water absorption behavior of hydrophobized concrete using silane emulsion as admixture, Cement and Concrete Research 154(2022) 106738.

[26] F. Wang, S. Lei, J. Ou, W. Li, Effect of pdms on the waterproofing performance and corrosion resistance of cement mortar, Applied Surface Science 507(2020) 145016.

[27] J. Song, D. Zhao, Z. Han, W. Xu, Y. Lu, X. Liu, B. Liu, C.J. Carmalt, X. Deng, I.P. Parkin, Super-robust superhydrophobic concrete, Journal of materials chemistry. A, Materials for energy and sustainability 5(2017) 14542-14550.

[28] J.B. Kardon, Polymer-modified concrete: review, Journal of Materials in Civil Engineering 9(1997) 85-92.

[29] D.W. Fowler, Polymers in concrete: a vision for the 21st century, Cement and Concrete Composites 21(1999) 449-452.

[30] N. Shirshova, A. Menner, G.P. Funkhouser, A. Bismarck, Polymerised high internal phase emulsion cement hybrids: macroporous polymer scaffolds for setting cements, Cement and Concrete Research 41(2011) 443-450.

[31] F. Wang, T. Xie, S. Lei, J. Ou, W. Li, M. Xue, D. Huang, Preparation and properties of foundry dust/Portland cement based composites and superhydrophobic coatings, Construction & building materials 246(2020) 118466.

[32] Z. Zhu, Z. Wang, Y. Zhou, Y. Wei, A. She, Synthesis and structure of calcium silicate hydrate (C-S-H) modified by hydroxyl-terminated polydimethylsiloxane (PDMS), Construction and Building Materials 267(2021) 120731.

[33] H. Yao, Z. Xie, C. Huang, Q. Yuan, Z. Yu, Recent progress of hydrophobic cement-based materials: preparation, characterization and properties, Construction and Building Materials 299(2021) 124255.

[34] S. Ruan, D. Yan, S. Chen, F. Jiang, W. Shi, Process and mechanisms of multi-stage water sorptivity in hydrophobic geopolymers incorporating polydimethylsiloxane, Cement and Concrete Composites 128(2022) 104460.

[35] A. Moshiri, D. Stefaniuk, S.K. Smith, A. Morshedifard, D.F. Rodrigues, M.J.A. Qomi, K.J.

Krakowiak, Structure and morphology of calcium-silicate-hydrates cross-linked with dipodal organosilanes, Cement and Concrete Research 133(2020) 106076.

[36] P. Gómez-Romero, C. Sanchez, Functional hybrid materials, John Wiley & Sons2006.

[37] S. Ruan, S. Chen, Y. Zhang, J. Mao, D. Yan, Y. Liu, X. Liu, H. Hosono, Molecular-level hybridized hydrophobic geopolymer ceramics for corrosion protection, Chemistry of Materials 35(2023) 1735-1744.

[38] J.L. Provis, S.A. Bernal, Geopolymers and related alkali-activated materials, Annual Review of Materials Research 44(2014) 299-327.

[39] Z. Guo, Q. Zhu, C. Liu, Z. Xing, Preparation of Ca-Al-Fe deicing salt and modified with sodium methyl silicate for reducing the influence of concrete structure, Construction and Building Materials 172(2018) 263-271.

[40] Q. Ma, S. Liu, Effect on silt capillary water absorption upon addition of sodium methyl silicate (SMS) and microscopic mechanism analysis, Coatings 10(2020) 724.

[41] D. Krenczkowska, K. Mojsiewicz-Pieńkowska, B. Wielgomas, K. Cal, R. Bartoszewski, S. Bartoszewska, Z. Jankowski, The consequences of overcoming the human skin barrier by siloxanes (silicones) part 1. Penetration and permeation depth study of cyclic methyl siloxanes, Chemosphere 231(2019) 607-623.

[42] R. Al-Oweini, H. El-Rassy, Synthesis and characterization by FTIR spectroscopy of silica aerogels prepared using several Si(OR)4 and R′′Si(OR′)3 precursors, Journal of Molecular Structure 919(2009) 140-145

[43] ASTM C1608-12. Standard test method for chemical shrinkage of hydraulic cement paste, in 2012.

[44] G. Fang, H. Bahrami, M. Zhang, Mechanisms of autogenous shrinkage of alkali-activated fly ash-slag pastes cured at ambient temperature within 24 h, Construction and Building Materials 171(2018) 377-387.

[45] ASTM C1698-09. Standard test method for autogenous strain of cement paste and mortar, in 2014.

[46] I. Ismail, S.A. Bernal, J.L. Provis, S. Hamdan, J.S.J. van Deventer, Drying-induced changes in the structure of alkali-activated pastes, Journal of Materials Science 48(2013) 3566-3577.

[47] V. Trincal, V. Benavent, H. Lahalle, B. Balsamo, G. Samson, C. Patapy, Y. Jainin, M. Cyr,

Effect of drying temperature on the properties of alkali-activated binders - recommendations for sample preconditioning, Cement and Concrete Research 151(2022) 106617.

[48] ASTM C1585-13. Standard test method for measurement of rate of absorption of water by hydraulic-cement concretes, in: West Conshohocken, PA 19428-2959. United States, 2013.

[49] R. Kurihara, I. Maruyama, Surface area development of portland cement paste during hydration: direct comparison with 1h nmr relaxometry and water vapor/nitrogen sorption, Cement and Concrete Research 157(2022) 106805.

[50] A. Assifaoui, D. Champion, E. Chiotelli, A. Verel, Characterization of water mobility in biscuit dough using a low-field 1h nmr technique, Carbohydrate Polymers 64(2006) 197-204.

[51] Z. Li, S. Zhang, Y. Zuo, W. Chen, G. Ye, Chemical deformation of metakaolin based geopolymer, Cement and Concrete Research 120(2019) 108-118.

[52] P. Duxson, A. Fernández-Jiménez, J.L. Provis, G.C. Lukey, A. Palomo, J.S.J. van Deventer, Geopolymer technology: the current state of the art, Journal of Materials Science 42(2007) 2917-2933.

[53] X. Zhu, D. Yan, H. Fang, S. Chen, H. Ye, Early-stage geopolymerization revealed by ^{27}Al and ^{29}Si nuclear magnetic resonance spectroscopy based on vacuum dehydration, Construction and Building Materials 266(2021) 121114

[54] L. Weng, K. Sagoe-Crentsil, Dissolution processes, hydrolysis and condensation reactions during geopolymer synthesis: Part I-Low Si/Al ratio systems, Journal of Materials Science 42(2007) 2997-3006

[55] E. Tazawa, S. Miyazawa, T. Kasai, Chemical shrinkage and autogenous shrinkage of hydrating cement paste, Cement and Concrete Research 25(1995) 288-292.

[56] V. Baroghel-Bouny, P. Mounanga, A. Khelidj, A. Loukili, N. Rafaï, Autogenous deformations of cement pastes: Part II. W/C effects, micro–macro correlations, and threshold values, Cement and Concrete Research 36(2006) 123-136

[57] L. Wu, N. Farzadnia, C. Shi, Z. Zhang, H. Wang, Autogenous shrinkage of high performance concrete: a review, Construction and Building Materials 149(2017) 62-75.

[58] J. Archez, R. Farges, A. Gharzouni, S. Rossignol, Influence of the geopolymer formulation on the endogeneous shrinkage, Construction and Building Materials 298(2021) 123813.

[59] D. Wang, C. Shi, Z. Wu, J. Xiao, Z. Huang, Z. Fang, A review on ultra high performance concrete:

part ii. Hydration, microstructure and properties, Construction and Building Materials 96(2015) 368-377.

[60] P. Duxson, G.C. Lukey, F. Separovic, J.S.J. van Deventer, Effect of alkali cations on aluminum incorporation in geopolymeric gels, Industrial & Engineering Chemistry Research 44(2005) 832-839.

[61] F. Lolli, J.J. Thomas, K.E. Kurtis, F. Cucinotta, E. Masoero, Early age volume changes in metakaolin geopolymers: insights from molecular simulations and experiments, Cement and Concrete Research 144(2021) 106428.

[62] G. Palumbo, A. Iadicicco, F. Messina, C. Ferone, S. Campopiano, R. Cioffi, F. Colangelo, Characterization of early age curing and shrinkage of metakaolin-based inorganic binders with different rheological behavior by fiber bragg grating sensors, Materials 11(2018)

[63] P. Mehta, P. Monteiro, Concrete: microstructure, properties, and materials, McGraw-Hill Education2014.

[64] K. Lum, D. Chandler, J.D. Weeks, Hydrophobicity at small and large length scales, The Journal of Physical Chemistry B 103(1999) 4570-4577.

[65] C. Hall, W.D. Hoff, Water transport in brick, stone and concrete, CRC Press2011.

[66] S. Park, M. Pour-Ghaz, What is the role of water in the geopolymerization of metakaolin? Construction and Building Materials 182(2018) 360-370.

[67] A.M. Gajewicz, Caracterisation of cement microstructure and pore-water interaction by 1 h nuclear magnetic resonance relaxometry, University of Surrey (United Kingdom)2014.

[68] A. Valori, P.J. McDonald, K.L. Scrivener, The morphology of C–S–H: lessons from 1h nuclear magnetic resonance relaxometry, Cement and Concrete Research 49(2013) 65-81.

[69] X. Hu, C. Shi, Z. Zhang, Z. Hu, Autogenous and drying shrinkage of alkali-activated slag mortars, Journal of the American Ceramic Society 102(2019) 4963-4975.

[70] P. Duxson, J.L. Provis, G.C. Lukey, F. Separovic, J.S.J. van Deventer, ^{29}Si NMR study of structural ordering in aluminosilicate geopolymer gels, Langmuir 21(2005) 3028-3036.

[71] D.H. Everett, IUPAC manual of symbols and terminology, appendix 2, part 1, colloid and surface chemistry, Pure and Applied Chemistry 31(1972) 578-621

[72] A.C.A. Muller, K.L. Scrivener, A.M. Gajewicz, P.J. McDonald, Densification of C–S–H measured by 1h NMR relaxometry, The Journal of Physical Chemistry C 117(2013) 403-412.

[73] T. Aly, J.G. Sanjayan, Mechanism of early age shrinkage of concretes, Materials and Structures 42(2008) 461.

[74] S.D. Beyea, B.J. Balcom, T.W. Bremner, P.J. Prado, A.R. Cross, R.L. Armstrong, P.E. Grattan-Bellew, The influence of shrinkage-cracking on the drying behaviour of White Portland cement using Single-Point Imaging (SPI), Solid State Nuclear Magnetic Resonance 13(1998) 93-100

[75] X. Zhu, H. Qian, H. Wu, Q. Zhou, H. Feng, Q. Zeng, Y. Tian, S. Ruan, Y. Zhang, S. Chen, D. Yan, Early-stage geopolymerization process of metakaolin-based geopolymer, Materials 15(2022) 6125.

[76] Z. Wu, H.S. Wong, C. Chen, N.R. Buenfeld, Anomalous water absorption in cement-based materials caused by drying shrinkage induced microcracks, Cement and Concrete Research 115(2019) 90-104.

[77] Y. Song, Z. Li, J. Zhang, Y. Tang, Y. Ge, X. Cui, A low-cost biomimetic heterostructured multilayer membrane with geopolymer microparticles for broad-spectrum water purification, ACS Applied Materials & Interfaces 12(2020) 12133-12142.

[78] H. Ma, H. Zhu, H. Chen, Y. Ni, X. Xu, Q. Huo, Shrinkage-reducing measures and mechanisms analysis for alkali-activated coal gangue-slag mortar at room temperature, Construction and Building Materials 252(2020) 119001.

[79] H. Ye, A. Radlińska, Shrinkage mechanisms of alkali-activated slag, Cement and Concrete Research 88(2016) 126-135.

[80] M. Hojati, F. Rajabipour, A. Radlińska, Drying shrinkage of alkali-activated cements: effect of humidity and curing temperature, Materials and Structures 52(2019) 118.